AGU100 ADVANCING EARTH AND SPACE SCIENCE

Geophysical Research Letters

RESEARCH LETTER
10.1029/2018GL080942

Key Points:
- We provide a comprehensive assessment of mass change for western North American (WNA) glaciers excluding those in Alaska
- WNA glaciers lost 117 +/- 42 gigatons (Gt) of mass over the period 2000-2018 and could account for 0.32 +/- 0.11 mm of sea level rise
- Regional changes in glacier mass are partly explained by decadal scale changes in atmospheric circulation

Supporting Information:
- Supporting Information S1

Correspondence to:
B. Menounos,
menounos@unbc.ca

Citation:
Menounos, B., Hugonnet, R., Shean, D., Gardner, A., Howat, I., Berthier, E., et al. (2019). Heterogeneous changes in western North American glaciers linked to decadal variability in zonal wind strength. *Geophysical Research Letters*, *46*, 200–209. https://doi.org/10.1029/2018GL080942

Received 15 OCT 2018
Accepted 7 DEC 2018
Accepted article online 13 DEC 2018
Published online 15 JAN 2019

Heterogeneous Changes in Western North American Glaciers Linked to Decadal Variability in Zonal Wind Strength

B. Menounos[1], R. Hugonnet[1,2], D. Shean[3], A. Gardner[4], I. Howat[5], E. Berthier[2], B. Pelto[1], C. Tennant[1], J. Shea[1], Myoung-Jong Noh[5], F. Brun[6], and A. Dehecq[4]

[1]Natural Resources and Environmental Studies Institute and Geography, University of Northern British Columbia, Prince George, British Columbia, Canada, [2]LEGOS, Université de Toulouse, CNES, CNRS, IRD, UPS, Toulouse, France, [3]Department of Civil and Environmental Engineering, University of Washington, Seattle, WA, USA, [4]Jet Propulsion Laboratory, California Institute of Technology, Pasadena, CA, USA, [5]School of Earth Sciences and Byrd Polar and Climate Center, The Ohio State University, Columbus, OH, USA, [6]Université Grenoble Alpes, CNRS, IRD, Grenoble INP, IGE, Grenoble, France

Abstract Western North American (WNA) glaciers outside of Alaska cover 14,384 km^2 of mountainous terrain. No comprehensive analysis of recent mass change exists for this region. We generated over 15,000 multisensor digital elevation models from spaceborne optical imagery to provide an assessment of mass change for WNA over the period 2000–2018. These glaciers lost 117 ± 42 gigatons (Gt) of mass, which accounts for up to 0.32 ± 0.11 mm of sea level rise over the full period of study. We observe a fourfold increase in mass loss rates between 2000–2009 [−2.9 ± 3.1 Gt yr^{-1}] and 2009–2018 [−12.3 ± 4.6 Gt yr^{-1}], and we attribute this change to a shift in regional meteorological conditions driven by the location and strength of upper level zonal wind. Our results document decadal-scale climate variability over WNA that will likely modulate glacier mass change in the future.

Plain Language Summary Glaciers in western North America provide important thermal and flow buffering to streams when seasonal snowpack is depleted. We used spaceborne optical satellite imagery to produce thousands of digital elevation models to assess recent mass loss for glaciers in western North America outside of Alaska. Our analysis shows that glacier loss over the period 2009–2018 increased fourfold relative to the period 2000–2009. This mass change over the last 18 years is partly explained by changes in atmospheric circulation. Our results can be used for future modeling studies to understand the fate of glaciers under future climate change scenarios.

1. Introduction

Anthropogenic warming is expected to drive continued mass loss from alpine glaciers throughout the remainder of this century (Marzeion et al., 2017). Relative to other alpine environments, glaciers in western North America (WNA) are expected to play a minor role in future sea level rise (Levermann et al., 2013; Marzeion et al., 2018; Radić et al., 2014) given their small, cumulative volume (Huss & Farinotti, 2012). These ice masses, however, represent important freshwater reservoirs that provide late-summer meltwater runoff when seasonal snowpacks have been depleted (Frans et al., 2018; Moore et al., 2009) or during years characterized by drought (Jost et al., 2012). Water managers require up-to-date assessments of how these ice masses have and will likely change in the coming decades.

A global assessment of glacier mass change by Gardner et al. (2013) included an estimate of WNA glacier mass loss of 14 ± 3 Gt yr^{-1} for the period 2003–2009 based on the extrapolation of sparse in situ surface mass balance (SMB) measurements (Cogley, 2009). Other approaches to estimate glacier mass change, such as satellite laser altimetry and satellite gravimetry employed by Gardner et al. (2013) for other glacierized regions, have so far proven unsuccessful for WNA due to sparse repeat-track spacing at lower latitudes and challenges associated with deconvolving competing mass change signals (groundwater, seasonal snow, reservoir volumes and glacio-isostatic adjustment). Such methods perform particularly poorly for lower-latitude mountain ranges with disperse glacier coverage, such as those that characterize WNA (Gardner et al., 2013; Jacob et al., 2012).

Repeat mapping of surface elevation through stereophotogrammetry provides an additional approach to measure glacier thickness change on a regional scale that can circumvent spatial and temporal biases imposed by using SMB observations to estimate regional mass change. Geodetic surveys exist for many

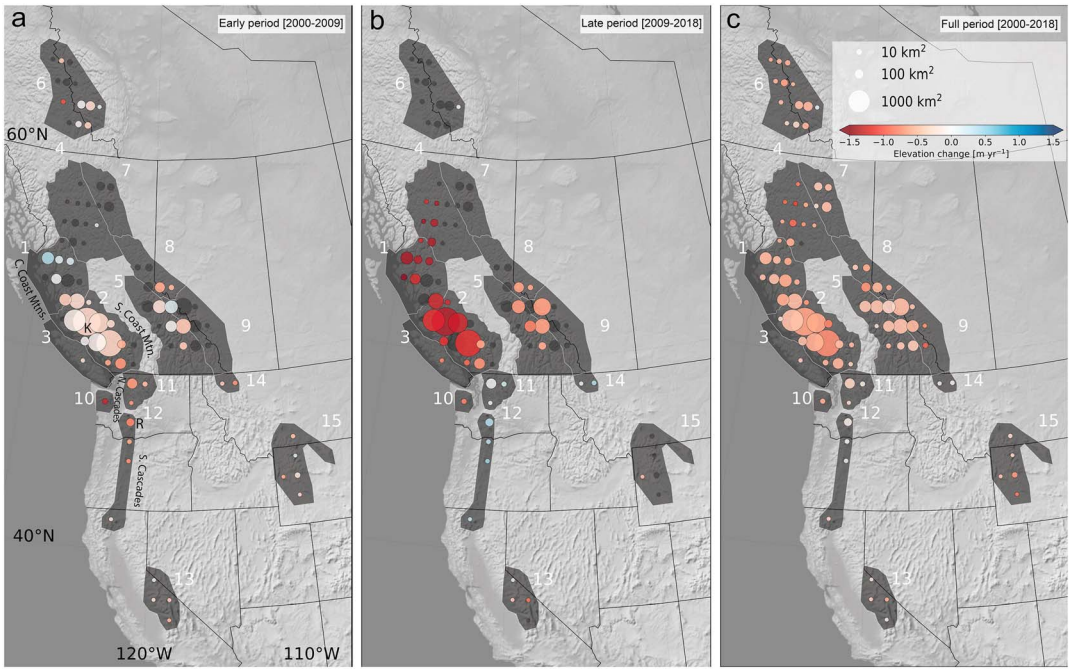

Figure 1. Gridded (1 × 1°) glacier elevation change (m yr^{-1}) for western North America. Circle diameters are scaled to area represented by grid point. Grid points with less than 30% of sampled ice are shown as dark gray. (a) early period (2000–2009), (b) late (2009–2018), (c) full (2000–2018). Numbers refer to subregions (Table 1) and letters "K" (region 03) and "R" (region 12) respectively denote approximate location of Klinaklini Glacier and Mount Rainier (Figure 2).

glacierized regions of WNA (e.g., Basagic & Fountain, 2011; Schiefer et al., 2007), but no study samples all of these regions in a systematic fashion. Novel methods to infer elevation change from medium resolution satellite imagery (Brun et al., 2017) coupled with automated processing of both medium and very high resolution optical satellite imagery (Noh & Howat, 2017; Shean et al., 2016) provide new opportunities to improve global estimates of glacier mass change.

The primary motivation of our paper is to provide the first, regionally complete estimate of glacier mass change for WNA for the period 2000–2018. We then use these data to (i) quantify the contribution of WNA glaciers to sea level rise over the last 18 years, (ii) determine the reliability and representativeness of existing WNA in situ SMB records, and (iii) assess the climatic drivers that affect mass change at the subregional scale.

2. Materials and Methods

Here we use the term WNA to define glaciers of Region 2 from the Randolph Glacier Inventory (RGI-6.0), which is the most comprehensive digital ice coverage map for WNA (RGI Consortium, 2017). Glaciers cover 14,384 km^2 of mountainous terrain in WNA with 88% of glacier coverage in British Columbia and Alberta, 7% in the conterminous United States (CONUS), and 5% in the Yukon and Northwest Territories (Figure 1 and Table 1). To provide regional comparisons of mass change, we subdivided glacierized terrain into 15 regions (Figure 1 and Table 1). In British Columbia, we use the same regions as those described in previous work (Clarke et al., 2015; Schiefer et al., 2007).

The primary data set we use to assess glacier mass change over the last 18 years consists of digital elevation models (DEMs) obtained from the Advanced Spaceborne Thermal Emission and Reflection Radiometer (ASTER) visible and near infrared instrument. The multispectral sensor collects both nadir and aft visible imagery with a native ground sample distance of 15 m and a swath width of ~60 km (Abrams, 2000; Raup et al., 2000). Our workflow for ASTER DEM generation (see supporting information S1) processes all ASTER scenes for 1 × 1° tiles that contain a minimum glacier area of 5 km^2. In British Columbia and Alberta, glacier extents in RGI-6.0 originate from Landsat imagery acquired between 2004 and 2006 (Bolch et al., 2010), whereas ice extents from Yukon, Northwest Territories, and CONUS originate from multiple sources with varied

Table 1
Elevation Change and Mass Budget of Western North American Glaciers (2000–2018)

Region	Area[a] (km^2)	Mass balance[b] (kg m^{-2} yr^{-1})			Mass budget (Gt yr^{-1})
		early[c]	late	full	full
Central Coast (1)[d]	1,580	−42 ± 221	−1,067 ± 418	−424 ± 163	−0.669 ± 0.258
Southern Coast (2)	7,180	−215 ± 190	−1,027 ± 258	−517 ± 140	−3.709 ± 1.006
Vancouver Island (3)	12	−205 ± 171	−681 ± 206	−309 ± 120	−0.004 ± 0.001
Northern Interior (4)	253	75 ± 298	−1,143 ± 510	−608 ± 222	−0.154 ± 0.056
Southern Interior (5)	1,946	−175 ± 232	−647 ± 352	−353 ± 185	−0.686 ± 0.360
Nahanni (6)	649	−220 ± 250	−419 ± 444	−407 ± 192	−0.264 ± 0.124
Northern Rockies (7)	415	−148 ± 271	−724 ± 506	−362 ± 233	−0.150 ± 0.097
Central Rockies (8)	422	−483 ± 284	−671 ± 370	−474 ± 202	−0.200 ± 0.086
Southern Rockies (9)	1,350	−200 ± 240	−614 ± 376	−394 ± 205	−0.533 ± 0.277
Olympics (10)	30	−1,113 ± 259	−696 ± 235	−474 ± 144	−0.014 ± 0.004
North Cascades (11)	250	−567 ± 184	46 ± 106	−245 ± 87	−0.061 ± 0.022
South Cascades (12)	153	−632 ± 147	346 ± 112	−46 ± 61	−0.007 ± 0.009
Sierra Nevada (13)	11	−234 ± 231	−448 ± 326	−318 ± 141	−0.004 ± 0.002
Glacier Natl. Park (14)	29	−522 ± 310	235 ± 268	−41 ± 158	−0.001 ± 0.005
Wind River (15)	60	−202 ± 249	−652 ± 571	−503 ± 187	−0.030 ± 0.011
Total (WNA)[e]	14,341	−203 ± 214	−858 ± 320	−452 ± 162	−6.49 ± 2.32

[a]Glacierized area. [b]Mass change (kg m^{-2} yr^{-1}) converted to mass using a density 850 kg m^{-3}. [c]Full, early, and late, respectively, refer to periods 2000–2009, 2009–2018, and 2000–2018. [d]Numbers refer to regions defined on Figure 1. [e]Area-weighted averages and uncertainties for mass balance.

acquisition dates (Fountain et al., 2017; Kienholz et al., 2015; Pfeffer et al., 2014). For the CONUS regions, all glacier outlines of the RGI-6.0 covering less than 0.1 km^2 were removed, which excludes less than 0.5% of all WNA ice cover from our analysis.

For DEM generation we used two open-source software packages for the mass production of DEMs from satellite stereoscopic imagery: the National Aeronautics and Space Administration Ames Stereo Pipeline (ASP) (Beyer et al., 2018; Shean et al., 2016) and the Ohio State University's Surface Extraction from TIN (triangulated irregular network)-based Search-space Minimization (SETSM; Noh & Howat, 2015, 2017). We used ASP to generate 15,500 DEMs with 30-m posting from ASTER stereoscopic imagery acquired between 2000 and 2018. We supplemented the ASTER DEMs with 693 higher-resolution (2 to 8 m) DEMs generated from submeter resolution DigitalGlobe WorldView-1, WorldView-2, WorldView-3, and GeoEye-1, and three DEMs generated from Pléiades satellite imagery (e.g., Berthier et al., 2014). WorldView/GeoEye data for CONUS were processed using ASP, while those over Canada were processed using SETSM. These non-ASTER DEMs, though temporally limited, increased repeat coverage for accumulation areas where ASTER DEMs often contain data gaps due to lack of surface texture at lower spatial and radiometric resolution. Their inclusion also increased sample count for trend fitting compared to the ASTER record.

Unlike many conventional geodetic mass balance studies that difference elevation data over glaciers between two epochs (e.g., Gardner et al., 2013; Schiefer et al., 2007), we evaluate per pixel linear trends for overlapping DEMs over the last 18 years (e.g., Willis et al., 2012). Our method builds upon the techniques described for glacier mass change in the French Alps (Berthier et al., 2016) and high-mountain Asia (Brun et al., 2017). We calculate the temporal trend in elevation (dh/dt) over stable and ice-covered terrain, the latter defined as those regions that lie within polygons of the RGI-6.0 glacier inventory. Time-variable glacier outlines are not available, so we use constant glacier area outlines for the full 18-year period (supporting information S1).

Individual DEMs were resampled to 30 m and coregistered over all stable, subaerial terrain excluding ice cover, and lakes (supporting information S1) using the Nuth and Kääb (2011) approach and the Global DEM (GDEMv2; Tachikawa et al., 2011) as a reference. Once DEMs are coregistered, we perform linear weighted least squares regression for a given map coordinate$_{\{x,\,y\}}$ with elevation $z_{\{t1,\,t2,\,\ldots,\,tn\}}$, where the subscript x,y refers to the local Universal Transverse Mercator projection easting and northing of a given DEM of time t. This method provides an estimate of elevation change (dh/dt) at coordinate$_{\{x,\,y\}}$ with associated error taken to be the confidence interval of the regression about the linear fit (supporting information S1). To

calculate volumetric change (dV/dt) for a given elevation band, we use hypsometric extrapolation where volume change is the summed product of average dh/dt for a given elevation band and its corresponding area. We use a density of 850 ± 60 kg m^{-3} to convert dV/dt to mass change (Huss, 2013). Global sea level equivalence is calculated using a density for water of 1,000 kg m^{-3} and an ocean surface area of 3.6×10^{14} m^2 (Amante, 2009).

Our uncertainty analysis consists of both random and systematic errors. Random errors are dominated by DEM quality (precision) and coregistration success; it can be approximated by the standard deviation (σ_z) of elevation change from stable surfaces corrected for spatial autocorrelation (Rolstad et al., 2009). Any seasonal elevation variability (e.g., snow cover and vegetation) is also included in this metric. Full details describing the propagation of errors, including systematic errors, are provided elsewhere (supporting information S1).

To calculate changes in rates of mass change at the decadal scale, we split the elevation data set into two epochs of equal duration [1 June 2000 to 15 September 2009 and 1 June 2009 to 15 September 2018] hereafter referred to as early [2000–2009] and late [2009–2018]. We did not consider changes in rates on timescales less than a decade because of relatively high errors in the individual ASTER DEMs and potentially insufficient temporal sampling.

We also analyzed geopotential height (500 hPa), temperature (700 hPa), precipitation, and wind (zonal, meridional, and speed) from ERA5 (Hersbach & Dee, 2016) for the two study epochs to evaluate climatological drivers for observed glacier mass change. The ERA5 is a global reanalysis product that consists of 107 vertical levels on a 31-km grid, assimilates the greatest number of surface- and satellite-based observations of any reanalysis product, and currently extends from January 2000 to August 2018. Temperature at 700 hPa is approximately 3,100 m above sea level, and so approximates air temperatures above the elevation of most glaciers in WNA. Interannual to interdecadal climate variability is known to affect mass change of WNA glaciers (Bitz & Battisti, 1999; Hodge et al., 1998; Moore et al., 2009; Watson et al., 2006), so we also evaluated whether decadal change in glacier mass were explained by any major shifts in ocean-atmospheric phenomena known to affect climate in WNA (supporting information S1).

3. Results

The DEMs cover over 99.5% of the WNA glacierized terrain, with statistically significant elevation change for 82% of those surveyed areas. Coverage for the early [2000–2009], late [2009–2018], and full periods [2000–2018] over glacierized terrain respectively averages 45% (10 DEMs per pixel), 45% (8 DEMs per pixel), and 80% (13 DEMs per pixel). Fortunately, the most heavily glacierized subregions of our study domain contain a suitable number of DEMs to minimize uncertainties for all three periods during the 1 × 1° tile aggregation. High random and systematic errors exist for some subregions (e.g., Olympic Mountains, Table 1) with limited available stable terrain for coregistration. We observe the highest uncertainty in the Interior Ranges and Canadian Rocky Mountains (Table 1) due to reduced temporal coverage (average of nine DEM samples per pixel). While some subregions, such as the Sierra Nevada, North Cascades, and South Cascades, have greater sample depth (26 DEMs per pixel on average), they still yield mass change estimates with moderate uncertainties due in part to the high errors caused by uncertainties in mapped glacier extent. Temporal subdivision increases the uncertainty in our mass change estimates due to the reduced sample size of each epoch relative to the full 2000–2018 period of study (supporting information S1).

We also calculated mass change using sequential DEM differencing of independent high-resolution data for 175 glaciers in British Columbia (Figure S1 and Table S1). Comparison of these changes over common periods of time suggests that our ASTER-based elevation trends (Figure S5) represent unbiased estimates of mass change for glaciers larger than 0.5 km^2 (supporting information S1).

WNA experienced spatially variable glacier elevation change over the period 2000–2018 (Figure 1). When elevation change is aggregated for subregions, small glaciers in the northern interior ranges of British Columbia thinned most, whereas our trend analysis is unable to detect elevation change that is statistically different from zero for glaciers within the South Cascades and Glacier National Park over the last 18 years (Figure 1 and Table 1). Large glaciers sourced from icefields in the southern Coast Mountains experienced high rates of thinning (> 10 m yr^{-1}) at low elevations (Figure 2). When averaged over all regions, WNA glaciers lost

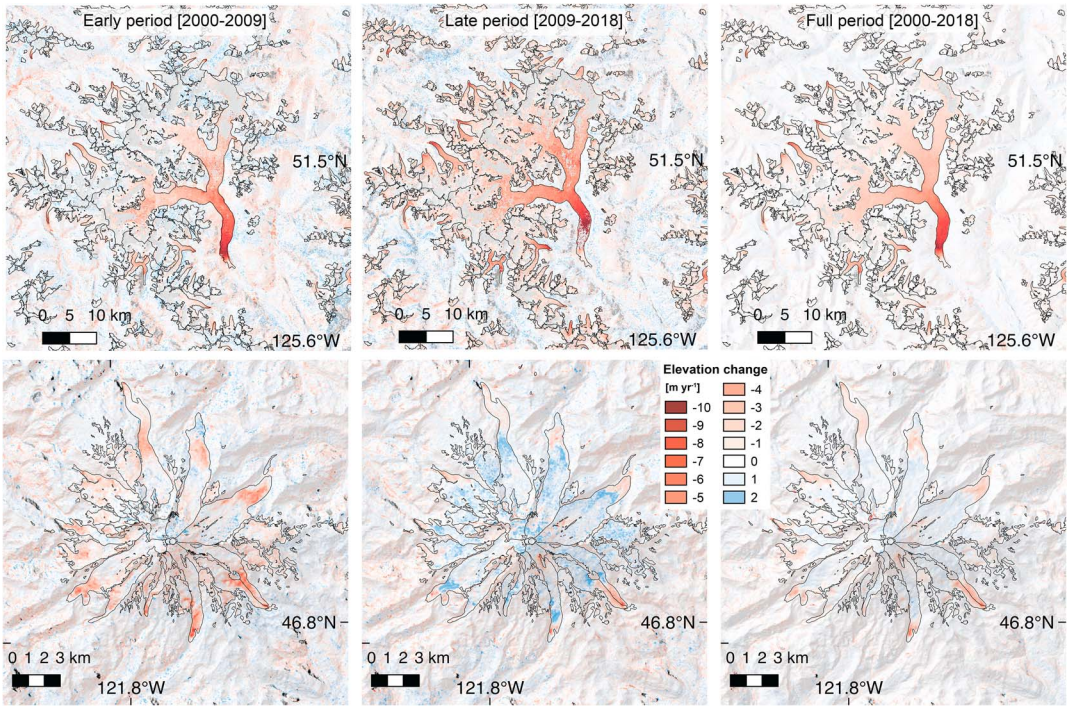

Figure 2. (top row) Elevation trend (m yr^{-1}) for Klinaklini Glacier (southern Coast Mountains) for early (top left), late (top middle), and full (top right). (bottom row) Same as upper row except for Mount Rainier (South Cascades). Gray areas denote no data.

-6.5 ± 2.3 Gt yr^{-1} during the period 2000–2018 (Table 1). Ninety-eight percent of this mass change originated from Canadian glaciers with ice loss in the southern Coast Mountains accounting for 58% of the total mass loss.

Our results show a fourfold increase in rates of mass loss between the early (-2.9 ± 3.1 Gt yr^{-1}) and late periods (-12.3 ± 4.6 Gt yr^{-1}), with notable regional differences (Figure 1). A prominent dipole in rates of mass change exists between the British Columbia central Coast [50–55°N] and the Cascade mountains [42–47°N] of the United States (Figure 1). During the early epoch, mass change was less negative for glaciers in the southern latitudes of British Columbia, whereas glaciers in the Cascade Mountains experienced high rates of mass loss (Table 1). This pattern reversed during the late period when glacier mass loss from the southern Coast Mountains increased by a factor of 4.8. Glaciers in the south Cascades showed slight mass gain with no detectable mass change in the north Cascades (Figure 2 and Table 1).

The ERA5 fields reveal changes in wind speed, temperature, and precipitation between the early and late periods (Figure 3). The north-south dipole in mass change along the U.S.-Canada border (Figure 1) coincide with a shift in the average location of the midlatitude jet, here defined as the maximum velocity for upper-level (250 hPa) winds. Regional composites of monthly averaged column-integrated moisture flux (kg·m^{-1}·s^{-1}), temperature (K) at 700 hPa, and precipitation (m yr^{-1}) over the early and late periods likewise reveal latitudinal differences in those meteorological conditions that influence SMB. Regional composites of geopotential height in the Northern Hemisphere also show a zone of lower than normal pressure across the latitude band [42–47°N] with an area of higher than normal pressure across most of British Columbia (supporting information S1). These differences in geopotential height are maximized for the winter season (October–May), but they also occur during summer (June–September). During the last decade wet conditions coincided with areas of lower-than-average geopotential height in the Pacific Northwest whereas the central Coast Mountains experienced warm, dry conditions (Figure 3).

An examination of the relation between meteorological conditions and glacier mass change at time scales finer than a decade is not possible given the number of DEMs required for statistically significant elevation trend analysis. Cumulative departures of monthly precipitation anomalies for the 31-km ERA5 grid cell near Mount Rainier in the North Cascades (Figure 2), however, reveals that the period 2000–2007 was

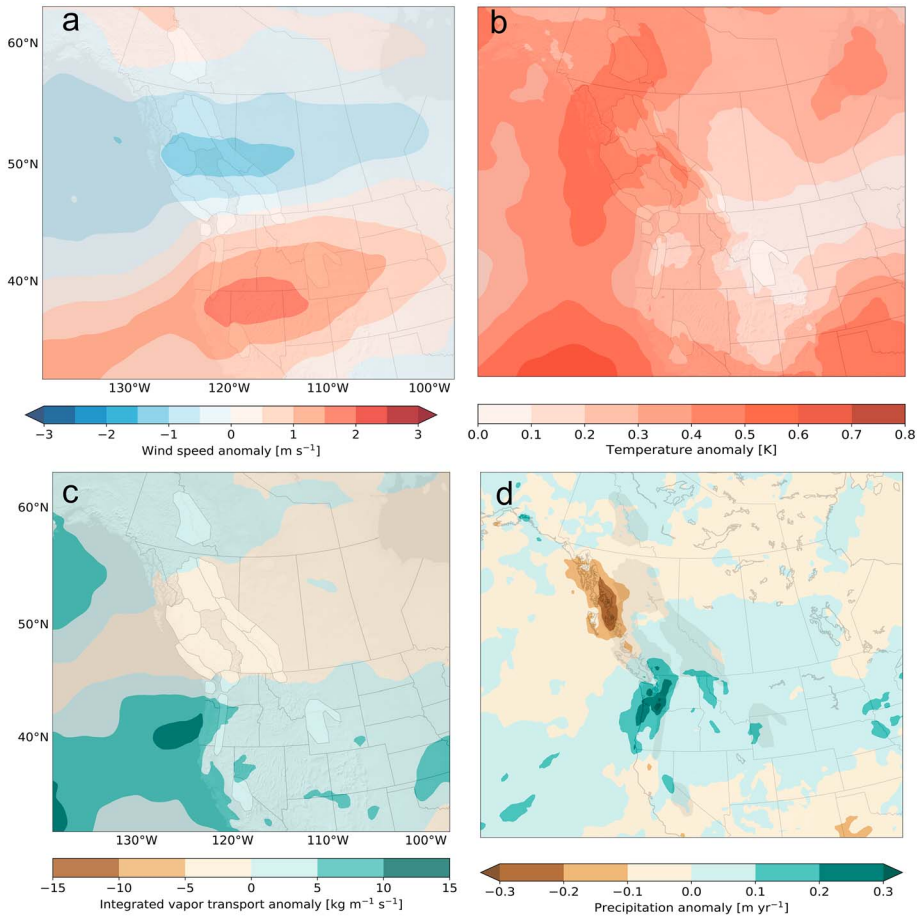

Figure 3. Anomalies ([2009–2017 mean] minus [2000–2009 mean]) of monthly fields from ERA5. (a) Zonal wind (250 hPa; m s^{-1}). (b) Temperature (700 hPa; K). (c) Column integrated vapor transport (kg m^{-1} s^{-1}). (d) Precipitation (m yr^{-1}).

characterized by drier than average conditions. An increase in precipitation commenced after 2011 for that location whereas a decrease in precipitation occurred over the central Coast Mountains after 2012.

Previous estimates of geodetic mass change for WNA glaciers at the subregional scale are primarily limited to British Columbia and Alberta (Schiefer et al., 2007). Our estimates and those from Schiefer et al. (2007) show a complex pattern of mass change (Figure 4), with most of these subregions showing mass loss for the period 1985–1999. Rates of mass loss slowed from 2000 to 2009 and then increased from 2009 to 2018 (Figure 4). The southern Coast Mountains alone contain nearly half of the total ice cover of WNA, and the rate of mass loss over the last 9 years was -7.4 ± 1.9 Gt yr^{-1}, about 20% faster than the period 1985–1999.

4. Discussion and Implications of Our Study

Our study provides a comprehensive assessment of glacier mass change (-6.5 ± 2.3 Gt yr^{-1}) for nearly all glacierized terrain in WNA over the period 2000–2018. Our estimated rate of WNA mass change for the early period (-2.9 ± 3.1 Gt yr^{-1}) is considerably less negative than the rate (-14 ± 3 Gt yr^{-1}) previously reported for the period 2003–2009 (Gardner et al., 2013).

In situ observations of SMB are invaluable given their temporal continuity and value in understanding climatic drivers of mass change (Hodge et al., 1998), but their use may bias regional estimates of mass change (Gardner et al., 2013). Our analysis (supporting information S1) shows that glaciological measurements of mass change are in broad agreement with geodetic estimates at the local scale, but they do not effectively sample large ice masses that dominate the regional signal of mass change from WNA, namely, large icefields in the southern Coast Mountains. Using available SMB measurements for 14 glaciers in WNA (supporting

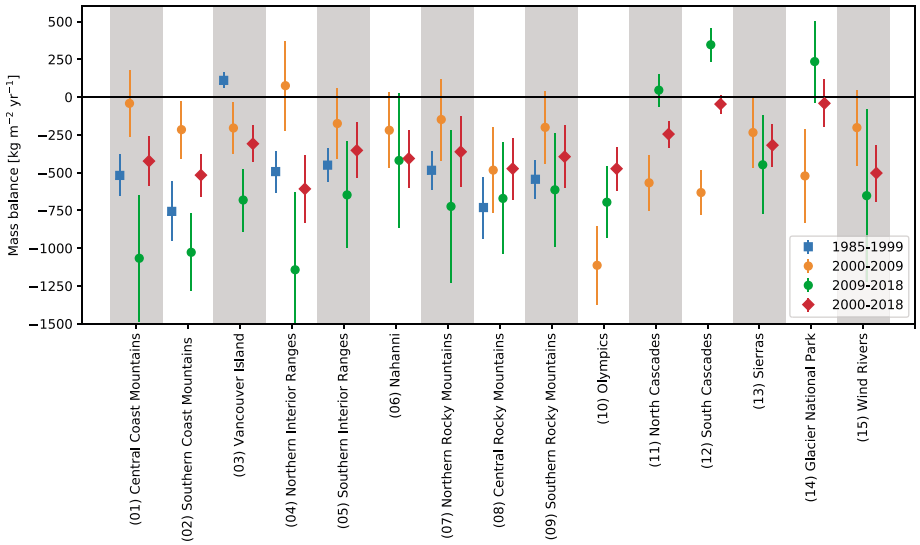

Figure 4. Estimated mass balance and uncertainties ($\pm 1\sigma$) for different subregions of western North American for periods 2000–2009, 2009–2018, 2000–2018, and for the period 1985–1999 (Schiefer et al., 2007).

information S1), we calculate an average mass change of -874 ± 100 kg m^{-2} yr^{-1} over the period 2000–2017. When multiplied by the total glacierized area of WNA, this value yields an annual mass loss of 13.6 ± 4.3 Gt yr^{-1}, close to the value (14 ± 3 Gt yr^{-1}) calculated by Gardner et al. (2013) using a similar approach. These values are twice as large as those based on our trend analysis. This discrepancy suggests that glaciers chosen for long-term monitoring programs are losing mass more rapidly than the region as a whole. Our findings accord with a study by Fountain et al. (2009), who concluded that South Cascade Glacier, chosen for long-term in situ SMB observations, lost three times more mass than glaciers in the north Cascade Mountains (subregion 11 of Table 1).

Cumulative mass loss from WNA glaciers over the period 2000–2018 could potentially account for 0.32 ± 11-mm global sea level rise equivalent, about 0.6% of observed SLR over the period 1993–2017 (Nerem et al., 2018). Our estimate is an upper limit as it assumes that meltwater from glacier mass loss was directly conveyed to the ocean and not stored in intermediate locations (e.g., proglacial lakes formed over the last 18 years). While surface storage of this water might be small, it could contribute to aquifer recharge (Liljedahl et al., 2017).

One of the most surprising findings of our study is the dipole pattern of mass change between glaciers in the British Columbia central Coast [50–55°N] and the Cascade mountains [42–47°N] of the United States (Figure 1). Positive anomalies in zonal winds (250 hPa) over the Cascade Mountains imply a strengthening and southward shift in the jet stream between the early and late periods that would increase the frequency of mid-latitude cyclones with attendant increases in precipitation. A change in meteorological conditions that favor changes in glacier mass are clearly revealed in the composite anomaly maps, especially for the central, southern Coast and Cascade glaciers (Figure 3). Glaciers of the southern Coast Mountains descend to lower elevations than those that flank high Cascade volcanoes. The partitioning of precipitation into either rain or snow may also explain why some of the Cascade glaciers gained mass during the recent period while Coast Mountain glaciers continued to experience strong thinning and mass loss. Future work employing surface mass and energy balance modeling at the glacier scale can be used to test this hypothesis.

The spatial distribution of subregional mass change is partly linked to regional changes in atmospheric circulation that affect accumulation and ablation. Others have noted the importance of zonal wind on controlling glacier mass balance (Marshall et al., 2011; Shea & Marshall, 2007), and some studies attribute a decline in zonal wind strength to explain the long-term (1950–2005) decline in winter snow water equivalent (Luce et al., 2013). In our study, anomalies in zonal wind covary with many of the meteorological fields known to control glacier mass balance, namely, temperature and precipitation. Orographically enhanced precipitation in WNA is also favored when strong zonal flow delivers moist air masses that originate over the Pacific Ocean

(Jarosch et al., 2012; Neiman et al., 2008). Regions of weak zonal wind also coincide with lower-than-average geopotential height over last 18 years.

It remains uncertain whether mass change observed over the last 18 years is related to natural climate variability known to affect glacier mass balance in WNA (Bitz & Battisti, 1999; Hodge et al., 1998; Moore & Demuth, 2001), stochastic variability, or whether these recent changes are related to anthropogenic climate change. We note no obvious relation between major climate indices and decadal changes in zonal wind strength or pressure at the subregional scale (supporting information S1). Using an ensemble of 25 global climate models, however, Luce et al. (2013) show that under a high emission scenario (RCP8.5), zonal wind (700 hPa) strength significantly decreases over the Cascade and Coast Mountains by the end of this century. Zonal winds weaken most over the central and southern Coast Mountains (50–55°N) but strengthen over southern latitudes of California (Luce et al., 2013). Based on the results of our study, weaker zonal winds would tend to favor stronger mass loss for glaciers in the Cascade and Coast Mountains.

Glaciers in both the CONUS and western Canada are expected to undergo continued mass loss throughout this century, even under moderate emission scenarios (Clarke et al., 2015; Frans et al., 2018; Huss & Hock, 2018). These changes will reduce or eliminate the thermal- and flow-buffering capacity provided by glacier runoff for many watersheds, with implications for downstream ecosystems and water resources. If the last 18 years provide a suitable analogue for the next 30–50 years, future glacier change will be modulated by decadal-scale climate variability. Like seasonal snow cover, improvement in understanding and forecasting climate variability at decadal time scales will be important to help guide estimates of glacier mass change for water management. Projections of future glacier mass change for both the CONUS (Frans et al., 2018) and western Canada (Clarke et al., 2015), like other regions, depend on well-distributed observations of glacier area and mass change, and our results can be used to improve modeling efforts that seek to understand the fate of glaciers under future climate scenarios.

Acknowledgments

This research was supported by grants from National Sciences and Engineering Research Council of Canada, the Canadian Foundation for Innovation, the Canadian Research Chairs Program, the Tula Foundation (Hakai Institute) and Global Water Futures (Water Mountain Futures), BC Hydro, and the Columbia Basin Trust. Gardner and Dehecq were supported by funding from the NASA Cryosphere and MEaSUREs Programs. Berthier acknowledges support from the French Space Agency (CNES) through the TOSCA program. The Pléiades stereo pairs were provided by the Pléiades Glacier Observatory initiative (CNES). SPOT 5 HRS DEMs were made available by the International Polar Year SPIRIT project (CNES). Shean acknowledges support from the National Park Service (NPS), United States Geological Survey (USGS), and National Aeronautics and Space Administration (NASA). Resources supporting the CONUS DEM production were provided by the NASA High-End Computing (HEC) Program through the NASA Advanced Supercomputing (NAS) Division at Ames Research Center. Menounos thanks NASA JPL for partial financial support during his sabbatical. DEM generation was supported by high-performance computer facilities at UNBC, Legos, Ohio State and the National Science Foundation. Howat and Noh were funded by the U.S. National Science Foundation Polar Cyberinfrastructure (PLR) program grant 1542736. WV DEMs for Canada were produced using an allocation from NSF Extreme Science and Engineering Discovery Environment (XSEDE). We acknowledge the agencies (World Monitoring Glacier Survey, the United States Geological Survey, and Natural Resources of Canada) and key individuals (Mike Demuth, Mark Ednie, Andrew Fountain, Ed Josberger, Bob Krimmel, Shad O'Neel, Mauri Pelto, Jon Riedel, Erin Whorton, and Gordon Young) for their efforts to establish and maintain monitoring programs for WNA glaciers. Data used in this contribution are available from http://www.unbc.ca/research/supplementary-data-unbc-publications. We thank an anonymous referee and Laura Thomson for providing detailed reviews that improved our manuscript. Finally, we wish to dedicate this study to the memory of Graham Cogley who passed away during the writing of this manuscript. Menounos, Gardner, Berthier, and Shean collectively designed the study; Hugonnet and Menounos processed the ASTER DEMs and completed the trend and uncertainty analysis; and Menounos wrote the initial draft of the paper. Pelto, Tennant, and Shea compiled and

References

Abrams, M. (2000). The Advanced Spaceborne Thermal Emission and Radiometer (ASTER): Data products for the high spatial resolution imager on NASA's Terra platform. *International Journal of Remote Sensing*, *21*(5), 847–859. https://doi.org/10.1080/014311600210326

Amante, C. (2009). *ETOPO1 1 arc-minute global relief model: procedures, data sources and analysis*. Washington, DC: National Ocean and Atmospheric Administration. Retrieved from http://www.ngdc.noaa.gov/mgg/global/global.htm

Basagic, H. J., & Fountain, A. G. (2011). Quantifying 20th century glacier change in the Sierra Nevada, California. *Arctic, Antarctic, and Alpine Research*, *43*(3), 317–330. https://doi.org/10.1657/1938-4246-43.3.317

Berthier, E., Cabot, V., Vincent, C., & Six, D. (2016). Decadal region-wide and glacier-wide mass balances derived from multi-temporal ASTER satellite digital elevation models. Validation over the Mont-Blanc area. *Frontiers of Earth Science*, *4*. https://doi.org/10.3389/feart.2016.00063

Berthier, E., Vincent, C., Magnússon, E., Gunnlaugsson, Á., Pitte, P., Le Meur, E., et al. (2014). Glacier topography and elevation changes derived from Pléiades sub-meter stereo images. *The Cryosphere*, *8*(6), 2275–2291. https://doi.org/10.5194/tc-8-2275-2014

Beyer, R. A., Alexandrov, O., & McMichael, S. (2018). The Ames Stereo Pipeline: NASA's open source software for deriving and processing terrain data. *Life Support & Biosphere Science: International Journal of Earth Space*, *56*, 221.

Bitz, C. M., & Battisti, D. S. (1999). Interannual to decadal variability in climate and the glacier mass balance in Washington, Western Canada, and Alaska. *Journal of Climate*, *12*(11), 3181–3196. https://doi.org/10.1175/1520-0442(1999)012<3181:ITDVIC>2.0.CO;2

Bolch, T., Menounos, B., & Wheate, R. (2010). Landsat-based inventory of glaciers in western Canada, 1985–2005. *Remote Sensing of Environment*, *114*(1), 127–137. https://doi.org/10.1016/j.rse.2009.08.015

Brun, F., Berthier, E., Wagnon, P., Kääb, A., & Treichler, D. (2017). A spatially resolved estimate of High Mountain Asia glacier mass balances, 2000-2016. *Nature Geoscience*, *10*(9), 668–673. https://doi.org/10.1038/ngeo2999

Clark, A., Fagre, D., Peitzsch, E., Reardon, B., & Harper, J. (2017). Glaciological measurements and mass balances from Sperry Glacier, Montana, USA, years 2005-2015. *Earth System Science Data*, *9*(1), 47–61. https://doi.org/10.5194/essd-9-47-2017

Clarke, G. K. C., Jarosch, A. H., Anslow, F. S., Radić, V., & Menounos, B. (2015). Projected deglaciation of western Canada in the twenty-first century. *Nature Geoscience*, *8*(5), 372–377. https://doi.org/10.1038/ngeo2407

Cogley, G., Adams, W., Ecclestone, M., Jung-Rothenhäusler, F., & Ommanney, C. S. L. (1996). Mass balance of White Glacier, Axel Heiberg Island, NWT, Canada, 1960–91. *Journal of Glaciology*, *42*(142), 548–563. https://doi.org/10.1017/S0022143000003531

Cogley, J. G. (2009). Geodetic and direct mass-balance measurements: Comparison and joint analysis. *Annals of Glaciology*, *50*(50), 96–100. https://doi.org/10.3189/172756409787769744

Demuth, M., & Keller, R. (2006). An assessment of the mass balance of Peyto Glacier (1966–1995) and its relation to recent and past-century climatic variability. Peyto Glacier: One century of. *Science*, *8*, 83–132.

Fountain, A. G., Glenn, B., & Basagic, H. J. (2017). The geography of glaciers and perennial snowfields in the American West. *Arctic, Antarctic, and Alpine Research*, *49*(3), 391–410. https://doi.org/10.1657/AAAR0017-003

Fountain, A. G., Hoffman, M. J., Granshaw, F., & Riedel, J. (2009). The "benchmark glacier" concept—Does it work? Lessons from the North Cascade Range, USA. *Annals of Glaciology*, *50*(50), 163–168. https://doi.org/10.3189/172756409787769690

Frans, C., Istanbulluoglu, E., Lettenmaier, D. P., Fountain, A. G., & Riedel, J. (2018). Glacier recession and the response of summer streamflow in the Pacific Northwest United States, 1960-2099. *Water Resources Research*, *54*, 772. https://doi.org/10.1029/2017WR021764

Gardner, A. S., Moholdt, G., Cogley, J. G., Wouters, B., Arendt, A. A., Wahr, J., et al. (2013). A reconciled estimate of glacier contributions to sea level rise: 2003 to 2009. *Science*, *340*(6134), 852–857. https://doi.org/10.1126/science.1234532

analyzed in situ data. Shean tasked, acquired, and processed WV imagery for the conterminous United States, while Gardner, Howat, Menounos and Noh acquired and processed WV scenes from western Canada. Brun and Dehecq developed code used in our analysis. All authors discussed and commented on the manuscript. Author contributions and competing interests: none.

Granshaw, F. D., & Fountain, A. G. (2006). Glacier change (1958–1998) in the North Cascades National Park Complex, Washington, USA. *Journal of Glaciology*, *52*(177), 251–256. https://doi.org/10.3189/172756506781828782

Hersbach, H., & Dee, D. (2016). ERA5 reanalysis is in production. *ECMWF Newsletter*, *147*, 7.

Hodge, S. M., Trabant, D. C., Krimmel, R. M., Heinrichs, T. A., March, R. S., & Josberger, E. G. (1998). Climate variations and changes in mass of three glaciers in western North America. *Journal of Climate*, *11*(9), 2161–2179. https://doi.org/10.1175/1520-0442(1998)011<2161:CVACIM>2.0.CO;2

Hopkinson, C., & Demuth, M. (2006). Using airborne lidar to assess the influence of glacier downwasting on water resources in the Canadian Rocky Mountains. *Canadian Journal of Remote Sensing*, *32*(2), 212–222. https://doi.org/10.5589/m06-012

Huss, M. (2013). Density assumptions for converting geodetic glacier volume change to mass change. *The Cryosphere*, *7*(3), 877–887. https://doi.org/10.5194/tc-7-877-2013

Huss, M., & Farinotti, D. (2012). Distributed ice thickness and volume of all glaciers around the globe. *Journal of Geophysical Research*, *117*(F4), F04010. https://doi.org/10.1029/2012JF002523

Huss, M., & Hock, R. (2018). Global-scale hydrological response to future glacier mass loss. *Nature Climate Change*, *8*(2), 135–140. https://doi.org/10.1038/s41558-017-0049-x

Jacob, T., Wahr, J., Pfeffer, W. T., & Swenson, S. (2012). Recent contributions of glaciers and ice caps to sea level rise. *Nature*, *482*(7386), 514–518. https://doi.org/10.1038/nature10847

Jarosch, A. H., Anslow, F. S., & Clarke, G. K. C. (2012). High-resolution precipitation and temperature downscaling for glacier models. *Climate Dynamics*, *38*(1–2), 391–409.

Josberger, E., Bidlake, W., March, R., & Kennedy, B. (2007). Glacier mass-balance fluctuations in the Pacific Northwest and Alaska, USA. *Annals of Glaciology*, *46*(1), 291–296. https://doi.org/10.3189/172756407782871314

Jost, G., Moore, R. D., Menounos, B., & Wheate, R. (2012). Quantifying the contribution of glacier runoff to streamflow in the upper Columbia River Basin, Canada. *Hydrology and Earth System Sciences*, *16*(3), 849–860. https://doi.org/10.5194/hess-16-849-2012

Kienholz, C., Herreid, S., Rich, J. L., Arendt, A. A., Hock, R., & Burgess, E. W. (2015). Derivation and analysis of a complete modern-date glacier inventory for Alaska and Northwest Canada. *Journal of Glaciology*, *61*(227), 403–420. https://doi.org/10.3189/2015JoG14J230

Korona, J., Berthier, E., Bernard, M., Rémy, F., & Thouvenot, E. (2009). SPIRIT. SPOT 5 stereoscopic survey of polar ice: Reference images and topographies during the fourth international polar year (2007–2009). ISPRS journal of photogrammetry and remote sensing: Official publication of the International Society for Photogrammetry and. *Remote Sensing*, *64*(2), 204–212.

Krimmel, R. (1999). Analysis of difference between direct and geodetic mass balance measurements at South Cascade glacier, Washington. *Geografiska Annaler. Series A, Physical Geography*, *81*(4), 653–658. https://doi.org/10.1111/j.0435-3676.1999.00093.x

Krimmel, R. M. (1997). Water, ice, meteorological, and speed measurements at South Cascade Glacier, Washington, 1996 balance year. *U.S. Geological Survey*. https://doi.org/10.3133/wri994049

Levermann, A., Clark, P. U., Marzeion, B., Milne, G. A., Pollard, D., Radic, V., & Robinson, A. (2013). The multimillennial sea-level commitment of global warming. *Proceedings of the National Academy of Sciences of the United States of America*, *110*(34), 13745–13750. https://doi.org/10.1073/pnas.1219414110

Liljedahl, A. K., Gädeke, A., O'Neel, S., Gatesman, T. A., & Douglas, T. A. (2017). Glacierized headwater streams as aquifer recharge corridors, subarctic Alaska. *Geophysical Research Letters*, *44*, 6876–6885. https://doi.org/10.1002/2017GL073834

Luce, C. H., Abatzoglou, J. T., & Holden, Z. A. (2013). The missing mountain water: Slower westerlies decrease orographic enhancement in the Pacific Northwest USA. *Science*, *342*(6164), 1360–1364. https://doi.org/10.1126/science.1242335

Marshall, S. J., White, E. C., Demuth, M. N., Bolch, T., Wheate, R., Menounos, B., et al. (2011). Glacier water resources on the eastern slopes of the Canadian Rocky Mountains. *Canadian Water Resources Journal/Revue Canadienne Des Ressources Hydriques*, *36*(2), 109–134. https://doi.org/10.4296/cwrj3602823

Marzeion, B., Champollion, N., Haeberli, W., Langley, K., Leclercq, P., & Paul, F. (2017). Observation-based estimates of global glacier mass change and its contribution to sea-level change. *Surveys in Geophysics*, *38*(1), 105–130. https://doi.org/10.1007/s10712-016-9394-y

Marzeion, B., Kaser, G., Maussion, F., & Champollion, N. (2018). Limited influence of climate change mitigation on short-term glacier mass loss. *Nature Climate Change*, *8*(4), 305–308. https://doi.org/10.1038/s41558-018-0093-1

Meier, M., & Tangborn, W. (1965). Net budget and flow of South Cascade Glacier, Washington. *Journal of Glaciology*, *5*(41), 547–566. https://doi.org/10.1017/S0022143000018608

Moore, R. D., & Demuth, M. N. (2001). Mass balance and streamflow variability at Place Glacier, Canada, in relation to recent climate fluctuations. *Hydrological Processes*, *15*(18), 3473–3486. https://doi.org/10.1002/hyp.1030

Moore, R. D., Fleming, S. W., Menounos, B., Wheate, R., Fountain, A., Stahl, K., et al. (2009). Glacier change in western North America: Influences on hydrology, geomorphic hazards and water quality. *Hydrological Processes*, *23*(1), 42–61. https://doi.org/10.1002/hyp.7162

Neiman, P. J., Ralph, F. M., Wick, G. A., Lundquist, J. D., & Dettinger, M. D. (2008). Meteorological characteristics and overland precipitation impacts of atmospheric rivers affecting the west coast of North America based on eight years of SSM/I satellite observations. *Journal of Hydrometeorology*, *9*(1), 22–47. https://doi.org/10.1175/2007JHM855.1

Nerem, R. S., Beckley, B. D., Fasullo, J. T., Hamlington, B. D., Masters, D., & Mitchum, G. T. (2018). Climate-change–driven accelerated sea-level rise detected in the altimeter era. *Proceedings of the National Academy of Sciences of the United States of America*, *115*(9), 2022–2025. https://doi.org/10.1073/pnas.1717312115

Noh, M. J., & Howat, I. M. (2017). The surface extraction from TIN based search-space minimization (SETSM) algorithm. *ISPRS Journal of Photogrammetry and Remote Sensing: Official Publication of the International Society for Photogrammetry and Remote Sensing*, *129*, 55–76.

Noh, M.-J., & Howat, I. M. (2015). Automated stereo-photogrammetric DEM generation at high latitudes: Surface extraction with TIN-based search-space minimization (SETSM) validation and demonstration over glaciated regions. *GIScience and Remote Sensing*, *52*(2), 198–217. https://doi.org/10.1080/15481603.2015.1008621

Nuth, C., & Kääb, A. (2011). Co-registration and bias corrections of satellite elevation data sets for quantifying glacier thickness change. *The Cryosphere*, *5*(1), 271–290. https://doi.org/10.5194/tc-5-271-2011

Pelto, M. (1996). Changes in glacier and alpine runoff in the North Cascade Range, Washington, USA 1985–1993. *Hydrological Processes*, *10*(9), 1173–1180. https://doi.org/10.1002/(SICI)1099-1085(199609)10:9<1173::AID-HYP368>3.0.CO;2-V

Pelto, M., & Brown, C. (2012). Mass balance loss of mount baker, Washington glaciers 1990–2010. *Hydrological Processes*, *26*(17), 2601–2607. https://doi.org/10.1002/hyp.9453

Pelto, M., & Riedel, J. (2001). Spatial and temporal variations in annual balance of North Cascade glaciers, Washington 1984–2000. *Hydrological Processes*, *15*(18), 3461–3472. https://doi.org/10.1002/hyp.1042

Pfeffer, W. T., Arendt, A. A., Bliss, A., Bolch, T., Cogley, J. G., Gardner, A. S., et al., & The Randolph Consortium (2014). The Randolph Glacier Inventory: A globally complete inventory of glaciers. *Journal of Glaciology*, *60*(221), 537–552. https://doi.org/10.3189/2014JoG13J176

Radić, V., Bliss, A., Cody Beedlow, A., Hock, R., Miles, E., & Graham Cogley, J. (2014). Regional and global projections of twenty-first century glacier mass changes in response to climate scenarios from global climate models. *Climate Dynamics*, *42*(1–2), 37–58.

Raup, B. H., Kieffer, H. H., Hare, T. M., & Kargel, J. S. (2000). Generation of data acquisition requests for the ASTER satellite instrument for monitoring a globally distributed target: Glaciers. *IEEE Transactions on Geoscience and Remote Sensing: A Publication of the IEEE Geoscience and Remote Sensing Society*, *38*(2), 1105–1112.

RGI Consortium (2017). Randolph Glacier Inventory—A dataset of global glacier outlines: Version 6.0: Technical report, Global Land Ice Measurements from Space, Colorado, USA. Digital Media. DOI: [Data set]. https://doi.org/10.7265/N5-RGI-60

Roberti, G., Friele, P., van Wyk de Vries, B., Ward, B., Clague, J. J., Perotti, L., & Giardino, M. (2017). Rheological evolution of the Mount Meager 2010 debris avalanche, southwestern British Columbia. *Geosphere*, *13*(2), 369–390.

Rolstad, C., Haug, T., & Denby, B. (2009). Spatially integrated geodetic glacier mass balance and its uncertainty based on geostatistical analysis: Application to the western Svartisen ice cap, Norway. *Journal of Glaciology*, *55*(192), 666–680. https://doi.org/10.3189/002214309789470950

Schiefer, E., Menounos, B., & Wheate, R. (2007). Recent volume loss of British Columbian glaciers, Canada. *Geophysical Research Letters*, *34*, L16503. https://doi.org/10.1029/2007GL030780

Shea, J. M., & Marshall, S. J. (2007). Atmospheric flow indices, regional climate, and glacier mass balance in the Canadian Rocky mountains. *International Journal of Climatology*, *27*(2), 233–247. https://doi.org/10.1002/joc.1398

Shean, D. E., Alexandrov, O., Moratto, Z. M., Smith, B. E., Joughin, I. R., Porter, C., & Morin, P. (2016). An automated, open-source pipeline for mass production of digital elevation models (DEMs) from very-high-resolution commercial stereo satellite imagery. *ISPRS Journal of Photogrammetry and Remote Sensing: Official Publication of the International Society for Photogrammetry and Remote Sensing*, *116*, 101–117.

Tachikawa, T., Hato, M., Kaku, M., & Iwasaki, A. (2011). Characteristics of ASTER GDEM version 2. In 2011 *IEEE International Geoscience and Remote Sensing Symposium* (pp. 3657–3660).

Tennant, C., & Menounos, B. (2013). Glacier change of the Columbia Icefield, Canadian Rocky Mountains, 1919–2009. *Journal of Glaciology*, *59*(216), 671–686. https://doi.org/10.3189/2013JoG12J135

Tennant, C., Menounos, B., Ainslie, B., Shea, J., & Jackson, P. (2012). Comparison of modeled and geodetically-derived glacier mass balance for Tiedemann and Klinaklini glaciers, southern Coast Mountains, British Columbia, Canada. *Global and Planetary Change*, *82–83*, 74–85.

VanLooy, J., & Forster, R. (2008). Glacial changes of five Southwest British Columbia icefields, Canada, mid-1980s to 1999. *Journal of Glaciology*, *54*(186), 469–478. https://doi.org/10.3189/002214308785836931

Watson, E., Luckman, B. H., & Yu, B. (2006). Long-term relationships between reconstructed seasonal mass balance at Peyto glacier, Canada, and Pacific sea surface temperatures. *Holocene*, *16*(6), 783–790. https://doi.org/10.1191/0959683606hol973ft

Willis, M. J., Melkonian, A. K., Pritchard, M. E., & Rivera, A. (2012). Ice loss from the Southern Patagonian Ice Field, South America, between 2000 and 2012. *Geophysical Research Letters*, *39*, L17501. https://doi.org/10.1029/2012GL053136

Young, G. J. (1981). The mass balance of Peyto glacier, Alberta, Canada, 1965 TO 1978. *Arctic and Alpine Research*, *13*(3), 307–318. https://doi.org/10.2307/1551037

Zemp, M., Nussbaumer, S., Gartner-Roer, I., Huber, J., Machguth, H., Paul, F., & Hoelzle, M. (2017). Global Glacier Change Bulletin (no. 2). World Glacier Monitoring Service, Switzerland.

Zemp, M., Thibert, E., Huss, M., Stumm, D., Rolstad Denby, C., Nuth, C., et al. (2013). Reanalysing glacier mass balance measurement series. *The Cryosphere*, *7*(4), 1227–1245. https://doi.org/10.5194/tc-7-1227-2013